DOI: 10.5937/ISAE25003W

ISAE 2025 - Book of Abstracts
The 7th International Symposium on Agricultural Engineering

Corresponding author ORCID: 0000-0002-3163-1548

STUDY OF SOIL–BASIN LISTER INTERACTION USING DISCRETE ELEMENT MODELLING APPROACH

Avdhoot Walunj*, Suyash Gadage, Abhishek Shinde, Sachin Nalawade

Dr. Annasaheb Shinde College of Agricultural Engineering and Technology, Mahatma Phule Krishi Vidyapeeth, Rahuri, Maharashtra, India-413722

*Corresponding author: aawalunj@gmail.com

Abstract: This study focuses on the study of soil–tool interaction using the Discrete Element Modelling (DEM) approach for a basin lister equipped with a watercourse attachment. The aim was to understand and predict the behavior of soil under varying operating speeds (2 km/h, 3 km/h, and 5 km/h) using Altair EDEM 2025. The basin lister geometry was modeled using Creo Parametric 11 and imported into the EDEM environment, where sandy clay loam soil was represented using bonded spherical particles (3–5 mm radius). The contact interactions were simulated using the Hertz-Mindlin with bonding model. Key performance indicators such as height and width of cross bunds, ridges, watercourses, and draft force were recorded. Model validation was carried out using the angle of repose and inclined plane tests. The simulation trends showed strong agreement with experimental results, with relative error ranging from 11.11% to 28.16% across parameters. The study demonstrates the reliability of DEM as a virtual test bench for tool development and performance optimization in tillage systems.

Keywords: Discrete Element Method (DEM), basin lister, soil–tool interaction, EDEM Simulation, Watercourse formation, Draft force.

1. Introduction

Mechanization in agriculture plays a crucial role in improving efficiency, conserving natural resources, and boosting productivity, especially in semi-arid and rainfed areas. Implements like basin listers are highly effective in forming rectangular basins and directing water into controlled channels, thus enhancing in-situ moisture conservation, and reducing soil erosion [1]. Traditional methods of evaluating tillage implements rely on field experiments, which are time-consuming, expensive, and prone to variability due to soil and environmental factors. This has led researchers to adopt simulation-based methods, notably the Discrete Element Method (DEM), to study soil–tool interactions in a virtual and controlled setting [2]. DEM simulates soil as an assembly of individual particles interacting through defined contact laws. It has been successfully used to investigate forces, soil movement, and tool performance in various tillage operations such as moldboard ploughing, chiseling, and subsoiling [3,4]. However, limited studies have explored its application to basin listers with integrated watercourse attachments for rectangular basin formation. This study focuses exclusively on the DEM-based simulation of a basin lister using Altair EDEM 2025. The tool geometry was developed in Creo Parametric 11, and the soil was modeled using bonded spherical particles to replicate the behavior of soil. Simulations were performed under different operating speeds, and parameters like bund height and width, ridge formation, watercourse shape, and draft force were analyzed. The DEM model was validated using angle of repose and inclined plane tests, as suggested by Obermayr et al. [5], ensuring accurate replication of particle behavior.

2. Materials and Methods

2.1. Basin Lister

A tractor-mounted, basin lister with watercourse attachment was used for trials, as shown in Fig. 1. The implement is designed to form micro-basins across the field for in-situ water conservation, while the watercourse attachment facilitates surface drainage. As the implement is pulled by a tractor, the watercourse attachment (ridger) engages the soil first, creating a shallow furrow that functions as a surface drain. Following this, the lister unit operates periodically (controlled by the stop and release mechanism) to form cross bunds by lifting and throwing soil laterally across the furrow. This results in discrete basins aligned with the furrow, spaced at regular intervals.

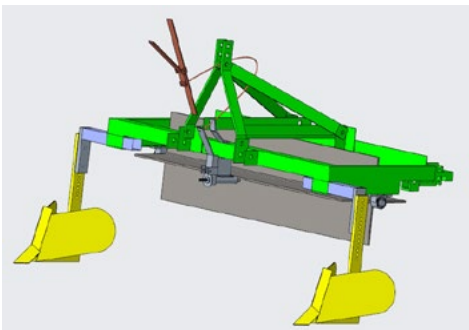

Figure 1 CAD Geometry of Basin Lister with watercourse attachment

Its main components include the main frame, lister unit, stop and release mechanism for lister unit, watercourse attachment (ridger) and hitch mast. The geometry was modeled in Creo Parametric 11 and exported into EDEM 2025.

2.2. Field conditions

The field soil was sandy clay loam, comprising 61.71% sand, 26.15% clay, and 12.14% silt. Soil samples were collected from 0–20 cm depth using the core cutter method, yielding an average moisture content (dry basis) of 13.84% and an average bulk density of 1490 kg/m³. Particle size distribution was assessed by passing air-dry soil through sieves ranging from 0.05 mm to 5 mm, with the highest particle distributions observed for 3 mm (19.28%) and 5 mm (12.01%) particles.

2.3. Discrete element modeling (DEM) simulations

The discrete element method (DEM) was employed to study soil-ridger interactions, with simulations run in Altair EDEM 2025. Computations were performed on a Dell Laptop with an Intel® Core i5 13th generation CPU @ 3170 GHz, Nvidia RTX 3050 6GB vRAM GPU and 16 GB of RAM.

2.3.1. Soil modeling

To ensure accurate and reliable simulation outcomes, constructing a representative soil particle model is crucial. In EDEM, particles are typically represented as spheres by default. However, using only spherical particles does not fully capture the complexity of real soil micro-aggregates. Prior research suggests that soil structures can be better modelled by grouping spherical particles into configurations such as lumps, columns, or nucleus-like assemblies as shown in Fig. 2. [7-9].

At present, there is no standardized guideline for determining soil particle sizes in discrete element simulations. Consequently, researchers typically select particle dimensions based on the number of particles required within the simulation domain and the limitations of available computational resources. A range of particle sizes has been employed in earlier soil-tool interaction studies, with a preference for spherical particles. For example, Ucgul et al. [10-12] utilized spherical particles with radii ranging from 5 mm to 10 mm in their analyses.

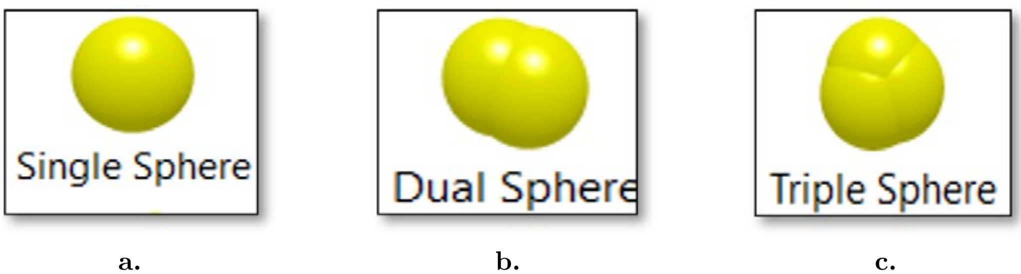

Figure 2 Soil particles shapes for soil bin development in EDEM a) Lump, b) Column, c) Nuclei

In this study, spherical particles with radii of 3 mm and 5 mm were used to model soil. These sizes were chosen considering the simulation domain's geometry and the performance constraints of the computing system. A combination of particle shapes and sizes was incorporated to represent the heterogeneity of soil structure more realistically. The proportions of the various soil particles used in the simulation are summarized in **Table 1.**

Table 1 Proportion of soil particles used in the simulation

Soil particle	Proportion %	No. of particles
3 mm single sphere	70.21	3266476
5 mm single sphere	19.84	923482
5 mm double sphere	7.63	355062
5 mm triple sphere	2.3	107339

2.3.2. Model parameters

The accuracy of a Discrete Element Method (DEM) simulation significantly depends on the selection of an appropriate contact model and the precise definition of DEM parameters. The contact model governs how particles behave upon interaction, while the base model describes the mechanics of particle-to-particle and particle-to-geometry collisions. According to Li et al. [13], cohesive interactions—such as liquid bridge bonding and inter-particle cohesion—play a critical role in influencing tillage resistance and the degree of soil disturbance. In alignment with their findings, the Hertz-Mindlin contact model with bonding was used in this study to replicate the cohesive nature of agricultural soils.

The parameters used in the DEM simulations are summarized in Table 2 and categorized into two groups: material parameters and contact parameters.

Material parameters include:

- Soil particle density,
- Poisson's ratio, and
- Shear modulus, for both the soil and the tool material (mild steel). Soil density was determined experimentally, while other values—such as the mechanical properties of mild steel and theoretical values for soil Poisson's ratio and shear modulus—were obtained from existing literature (Deng et al., 2016). The shear modulus (G) of mild steel was computed using the following relation:

$$G = E / 2(1 + \upsilon) \qquad (1)$$

where,
G is the shear modulus (Pa);
E is the elastic modulus (Pa); and
υ is Poisson's ratio.

Contact parameters include the coefficient of restitution, the coefficient of static friction, and the coefficient of rolling friction for soil particles and soil-tool interactions.

The static friction coefficients were determined experimentally through angle of repose and inclined plane tests, while the coefficient of restitution and rolling friction coefficients were obtained from literature [14]. Additional calibration support for these values was drawn from Fang et al. [15], who conducted systematic testing of soil frictional behaviour.

Table 2 DEM input parameters

Parameters	Value
Radius of the filling element, r (mm)	3 and 5
Soil particle density, ρ1 (kg/m3)	1490
Poisson's ratio of the soil particles, υ1	0.4
Shear modulus of the soil particles, G1 (Pa)	1×106
Poisson's ratio of Mild steel, υ2	0.30
Shear modulus of Mild steel, G2 (Pa)	1×1010
Density of Mild steel, ρ2 (kg/m3)	7800
Coefficient of restitution between soil and soil, e1	0.6
Coefficient of rolling friction between soil and soil, e2	0.2
Coefficient of static friction between soil and soil, e3	0.57
Coefficient of restitution between soil and Mild steel, f¬1	0.3
Coefficient of rolling friction between soil and Mild steel, f¬2	0.05
Coefficient of static friction between soil and Mild steel, f¬3	0.5
Percentage of the Rayleigh Time Step %	20
Simulation time, t (s)	5

In EDEM, the time step controls how frequently interaction calculations are performed during the simulation. This step size is typically defined as a percentage of the Rayleigh time step, which represents the time it takes for a shear wave to propagate through a particle. Based on software recommendations, this study used a time step equivalent to 20% of the Rayleigh time step.

The Rayleigh time step (Tr) was computed using the following equation:

$$Tr = \frac{\pi R \sqrt{\frac{\rho}{G}}}{0.1631\ \upsilon + 0.8766} \tag{2}$$

where,
R is the particle radius,
ρ is the particle density,
υ is the Poisson's ratio and
G is the particle shear modulus.

2.3.3. Model validation

The angle of repose (AOR) is a key parameter representing the steepest angle at which a mass of soil remains stable without sliding, measured with respect to the horizontal plane. It is typically calculated using the height and diameter of a soil heap formed naturally on a flat surface.

Among several established methods to determine AOR, the lifting cylinder technique is widely accepted for its simplicity and accuracy [16]. In this study, a vertical funnel with an upper diameter of 265 mm, a lower opening of 50 mm, and a height of 350 mm was used. The funnel was filled with soil to a height of 325 mm and lifted vertically at a constant speed of 0.05 m/s. This allowed the soil to form a conical pile on a flat platform. The test was repeated three times to obtain an average AOR value for sandy clay loam soil at a moisture content of 13.84% (dry basis).

To validate the soil model used in the simulation, the same test setup was replicated in Altair EDEM. The simulated particles were allowed to form a similar heap under gravitational influence to determine the soil's repose angle digitally.

The angle of repose was found to be 30° in both the physical and virtual experiments, indicating that the simulated soil behaviour closely matched real-world conditions. This validation supports the reliability of the DEM particle configuration used in this study. The visual comparison of both test results is illustrated in **Fig. 3.**

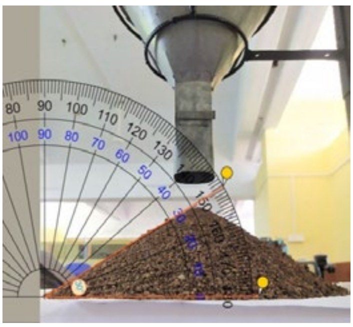

a.

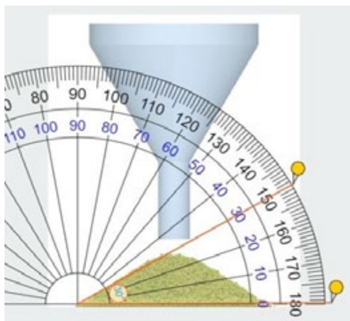

b.

Figure 3 Angle of repose test a) Laboratory test for field soil and b) Test in EDEM software for prepared soil

2.3.4. Soil-basin lister modeling

A three-dimensional (3D) CAD model of the basin lister equipped with a watercourse attachment was developed using Creo Parametric 11, maintaining a 1:1 scale to ensure geometric accuracy. This model was then imported into Altair EDEM 2025, where a virtual soil bin was constructed with dimensions of 3000 mm in width, 2000 mm in length, and 400 mm in height, as illustrated in Fig. 4. These dimensions were selected to facilitate the analysis of soil behaviour under varying tillage depths and forward speeds.

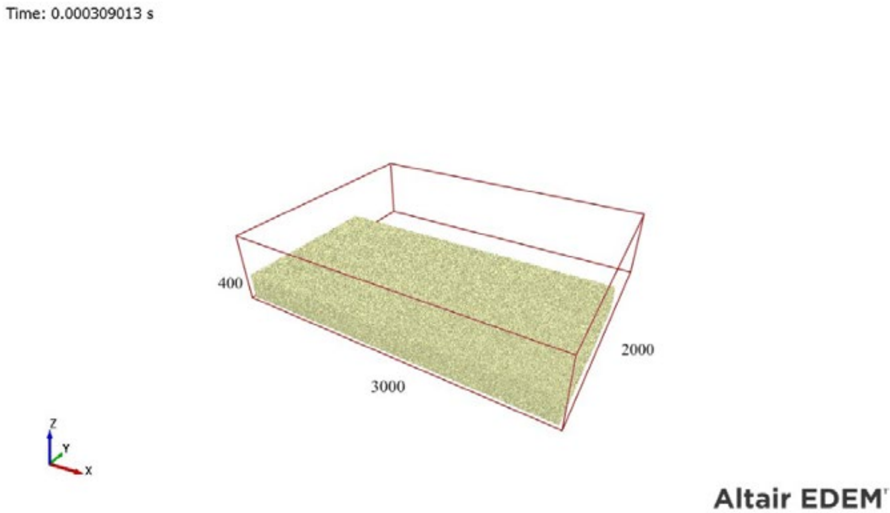

Figure 4 Soil bin in EDEM Software

During the simulation, key performance parameters such as draft force and soil disturbance characteristics—including cross bund height, cross bund width, side ridge height, side ridge width, watercourse depth, and watercourse width—were monitored using the same measurement methodology as employed in the physical experiments.

To evaluate the accuracy of the DEM simulations, relative error (RE) between the simulated outputs and the experimentally measured values was calculated using the following equation, adapted from Chen et al. (2013):

$$\text{RE}\ (\%) = \frac{M - S}{M} \times 100 \quad (3)$$

where,
RE is relative error (%)
M is measured value
S is simulation value

3. Results and Discussion

3.1 Cross bund height

Fig. 5 shows the variation in cross bund height with respect to operational speed (2 km/h, 3 km/h, and 5 km/h). Cross bund height is defined as the vertical distance between the top of the cross bund and the basin level. It is influenced by the speed of operation of the implement.

It is observed that cross bund height increases with increasing speed. At higher speeds, the lister blade interacts with the soil more aggressively, resulting in greater lifting of soil particles and their deposition at higher altitudes. There is also an increase in the kinetic energy imparted to the soil particles. The excess laterally scattered soil particles generated by the watercourse attachment (ridger) are subsequently carried by the lister blade, resulting in greater soil volume displacement.

The maximum cross bund height of 161 mm is achieved at a forward speed of 5 km/h, while the minimum height of 136 mm is recorded at 2 km/h. The available experimental data also reveal the same trend—an increase in bund height with increasing forward speed. These results highlight the tool's efficiency at high speeds for bund development but also caution that excessive soil scattering could occur in field scenarios without boundary control.

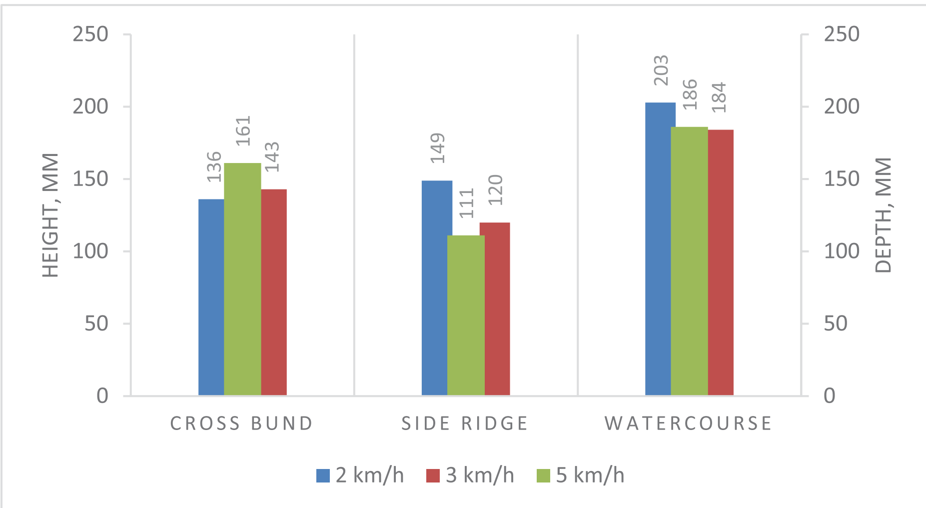

Figure 5 Effect of operating speed on height/depth

3.2. Cross bund width

Fig. 6 shows the variation in cross bund width with respect to operational speed (2 km/h, 3 km/h, and 5 km/h). Cross bund width is defined as the horizontal distance between the lowest points of the bund on both sides.

It is observed that cross bund width remains relatively unchanged or increases slightly at very high operating speeds. The experimental data available for the study also exhibit a similar trend, showing a slight increase in cross bund width as operating speed increases. These results indicate that an optimum operating speed must be considered to achieve the desired bund profile without excessive soil dispersion.

Figure 6 Effect of operating speed on width

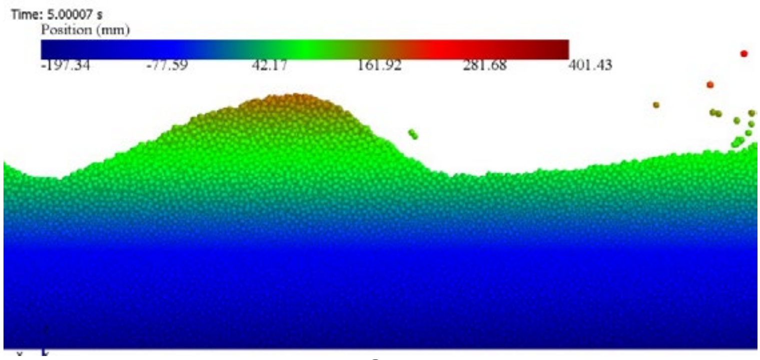

a.

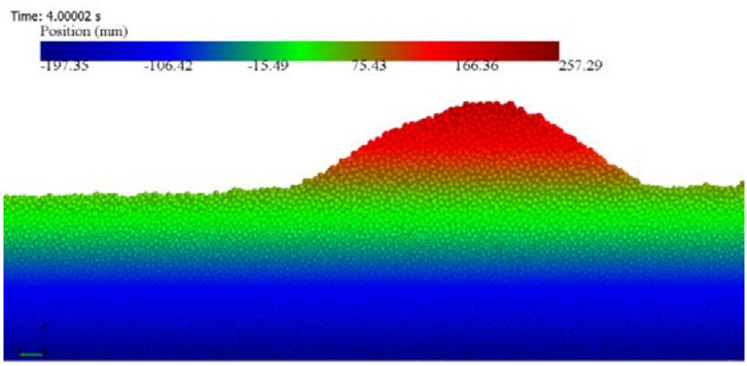

b.

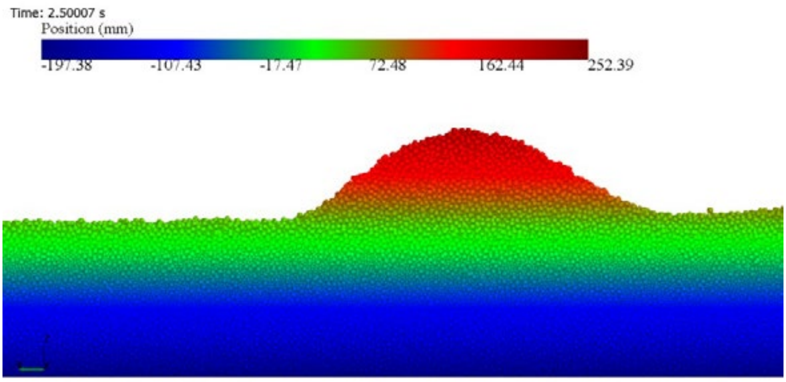

c.

Figure 8 Cross bund profile at a) 2 kmph, b) 3 kmph, c) 5 kmph speed of operation for DEM simulation

3.3. Side ridge height

Fig. 5 shows the variation in side ridge height with respect to operational speed (2 km/h, 3 km/h, and 5 km/h). Ridge height is defined as the vertical distance between the top of the side ridge and the basin level.

It is observed that ridge height decreases with an increase in operating speed. This decreasing trend is attributed to the greater velocity imparted to the soil particles at higher speeds. As the particles are displaced laterally, the increased velocity results in more widespread scattering of soil, preventing the formation of tall ridges.

A maximum ridge height of 149 mm is achieved at 2 km/h, while a minimum of 111 mm is observed at 5 km/h. A similar trend is observed in the experimental data.

3.4. Side ridge width

Fig. 6 shows the variation in side ridge width with respect to operational speed (2 km/h, 3 km/h, and 5 km/h). Ridge width is defined as the horizontal distance between the two ends of the ridge at the basin level.

It is observed that ridge width increases with increasing operational speed, reaching a peak at 3 km/h, and then begins to decrease at higher speeds. This decrease is caused by irregular soil throw patterns at high speeds, which narrow the ridge slightly. Another notable observation is that the excess laterally scattered soil particles are carried forward by the lister plate, resulting in minimal change in ridge width even at higher speeds.

The maximum ridge width of 289 mm is achieved at 3 km/h, while the minimum of 265 mm is recorded at 2 km/h. An increasing trend in ridge width is also observed in the experimental data.

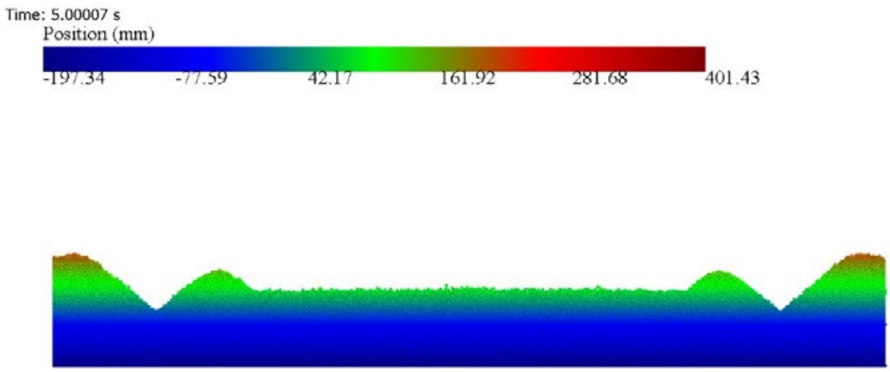

a.

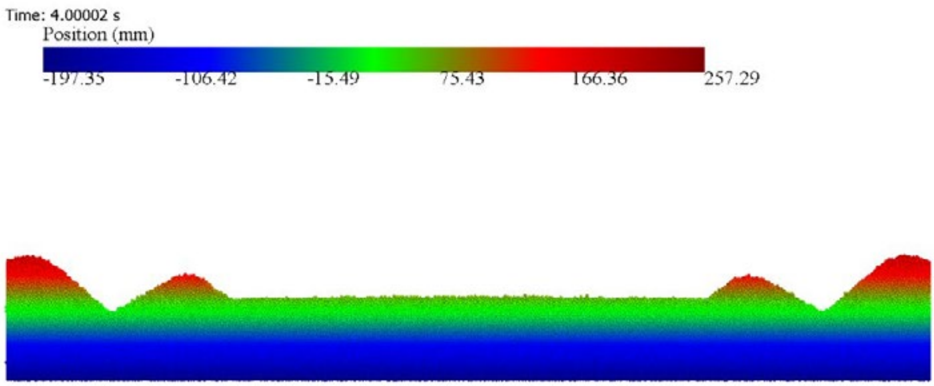

b.

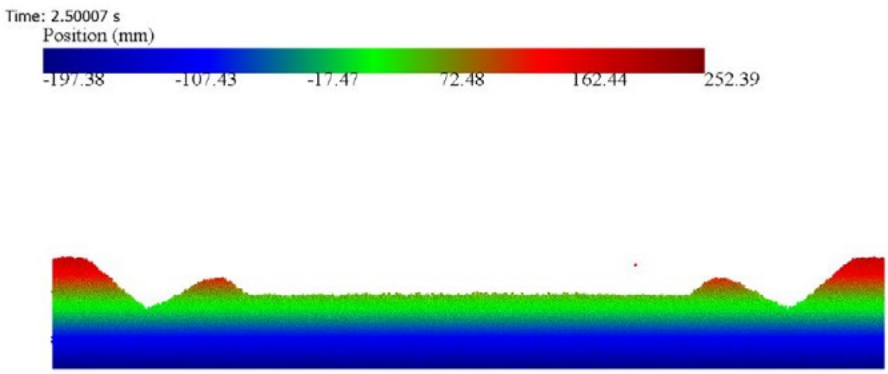

c.

Figure 9 Side Ridge and Watercourse profile at a) 2 kmph, b) 3 kmph, c) 5 kmph speed of operation for DEM simulation

3.5. Watercourse depth

Fig. 5 shows the variation in watercourse depth with respect to operational speed (2 km/h, 3 km/h, and 5 km/h). Watercourse depth is defined as the vertical distance between the bottom-most point of the watercourse and the top of the ridge formed alongside it.

It is observed that watercourse depth decreases with increasing speed and remains relatively constant at higher speeds. This reduction is attributed to insufficient tool penetration time at higher speeds. At slower speeds, the implement has more time to penetrate and carve the soil downward, creating a deeper watercourse. In contrast, faster speeds compromise the time available for effective cutting action, leading to shallower and less defined channels.

The maximum watercourse depth of 230 mm is recorded at 2 km/h, and the minimum of 184 mm at 3 km/h. A similar decreasing trend is observed in the experimental data.

3.6. Watercourse width

Fig. 6 shows the variation in watercourse width with respect to operational speed (2 km/h, 3 km/h, and 5 km/h). Watercourse width is defined as the horizontal distance between the top-most points of the watercourse.

It is observed that watercourse width increases with the increase in operating speed. The broader width at higher speeds is due to increased soil momentum, which spreads the particles more widely across the field surface. Although higher speeds enable broader coverage, they also lead to flatter and shallower watercourses, which may reduce water retention efficiency.

The maximum watercourse width of 540 mm is recorded at 5 km/h, and the minimum of 510 mm at 2 km/h. A similar trend is observed in the experimental data.

3.7. Draft

Fig. 7 shows the variation in draft force with respect to operational speed (2 km/h, 3 km/h, and 5 km/h). Although the draft force has generally increased with speed, this increase has not followed a strictly linear pattern. From 2 km/h to 3 km/h, the draft force has shown a substantial rise, increasing from 430.27 kgf to 561.38 kgf. However, the further increase to 588.57 kgf at 5 km/h has been comparatively marginal.

This non-linear behaviour is attributed to several interrelated mechanical and simulation-based factors. The first factor is increased soil scattering: at higher speeds, soil is thrown more laterally due to increased kinetic energy. This lateral movement has prevented the accumulation of soil directly in front of the implement. Without a dense resistance front, the tool has encountered lower passive pressure, reducing the draft load despite the increase in speed.

The second factor is reduced tool–soil contact time at high speeds. As speed increases, the contact duration between the lister blade and soil particles decreases, limiting the time available for penetration and engagement. Consequently, less soil is displaced per unit of contact, and the resistance force tends to plateau instead of rising proportionally with speed.

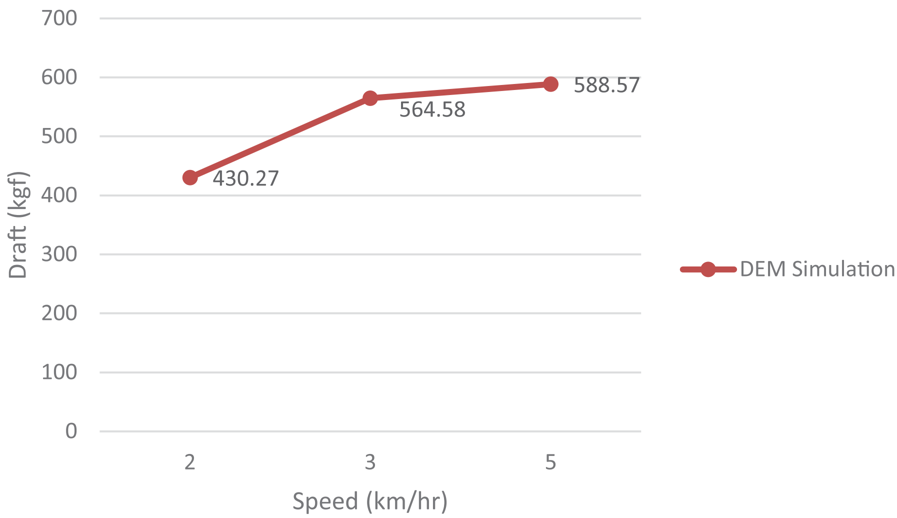

Figure 7 Effect of operating speed on draft

The third factor is the limitations of the DEM model to replicate the real-life soil conditions, resulting in the unexpected change in the trend.

A similar trend has been confirmed through experimental studies.

3.8. Relative Error

The relative error between the experimental values and the DEM-simulated results was calculated for various parameters at different operating speeds (2 km/h and 3 km/h). The relative error provides a quantitative assessment of the accuracy and validity of the DEM model by comparing it against field-tested values. Tab. 4 presents the relative error between the experimental data and DEM simulation results.

Tab. 4 Relative error between Experimental and DEM simulation study

SN	Speed km h^{-1}	Error, %						
		Height of Cross Bund	Width of Cross Bund	Height of Side Ridge	Width of Side Ridge	Depth of Water-course	Width of Water-course	Draft
1	2	11.11	17.31	24.16	19.69	12.5	17.87	28.16
2	3	14.88	24.93	16.50	18.13	13.61	19.78	12.05

The relative error for cross bund height ranged from 11.11% at 2 km/h to 14.88% at 3 km/h, while the error for cross bund width increased from 17.31% to 24.93%. For side ridge height, the relative error decreased from 24.16% at 2 km/h to 16.50% at 3 km/h.

Similarly, side ridge width showed a small variation in error, reducing from 19.69% to 18.13%.

In terms of watercourse dimensions, the relative error for depth increased slightly from 12.50% to 13.61%, while the width error rose from 17.87% to 19.78% as speed increased. The relative error for draft force showed the highest variation, decreasing from 28.16% at 2 km/h to 12.05% at 3 km/h.

4. Conclusions

The research on the Discrete Element Modelling (DEM) of soil–basin lister interactions has provided meaningful insights into the effects of operating speed on performance parameters such as cross bund height and width, side ridge formation, watercourse profile, and draft force. The following conclusions are drawn from this study:

- The cross bund height has shown an increasing trend with speed, ranging from 136 mm at 2 km/h to 161 mm at 5 km/h, due to enhanced soil uplift and lateral soil movement carried by the lister blade.
- The cross bund width has remained relatively stable but has shown a slight increase at higher speeds. It ranged from 651 mm at 2 km/h to 620 mm at 5 km/h, indicating that bund width is less sensitive to speed variations compared to height.
- The side ridge height decreased consistently with increased speed. The maximum ridge height of 149 mm was recorded at 2 km/h, reducing to 111 mm at 5 km/h, due to reduced soil deposition and increased lateral scattering at higher kinetic energy levels.
- The side ridge width increased up to 289 mm at 3 km/h but dropped slightly to 270 mm at 5 km/h, suggesting an optimum range of operating speed for maximum ridge width without over-scattering of soil.
- The watercourse depth decreased with increasing speed, from 230 mm at 2 km/h to 184 mm at 3 km/h, and remained nearly constant thereafter, reflecting a reduction in penetration effectiveness at higher forward velocities.
- The watercourse width increased with speed, ranging from 510 mm at 2 km/h to 540 mm at 5 km/h, showing that higher speeds cause greater lateral displacement of soil in the watercourse region.
- The draft force increased non-linearly, with values ranging from 430.27 kgf at 2 km/h to 588.57 kgf at 5 km/h. The increase from 3 km/h to 5 km/h was comparatively smaller, attributed to reduced soil-tool engagement and soil deflection behaviour in the DEM environment.
- The maximum relative error between experimental and DEM simulated values for the observed parameters was found to be 14.88% for cross bund height, 24.93% for cross bund width, 24.16% for side ridge height, 19.69% for side ridge width, 13.61% for watercourse depth, 19.78% for watercourse width, and 28.16% for draft force. These values confirm the reliability of the DEM model within acceptable simulation accuracy limits.

References

[1] Nimje, V. S., Jayanthi, A., & Patil, M. G. V. Performance evaluation of basin lister for semi-arid regions. Soil & Tillage Research, 134, 12–20, 2014.
[2] Cundall, P. A., & Strack, O. D. L. A discrete numerical model for granular assemblies. Géotechnique, 29(1), 47–65, 1979.
[3] Fielke, B. Interaction of the cutting edge of tillage implements with soil. Soil & Tillage Research, 97(1), 68–77, 2007.
[4] Chen, Y., Lobb, T. C., & Rahman, S. Soil disturbance and draft forces of tillage tools in cohesive soils. Biosystems Engineering, 85(1), 135–143, 2003.
[5] Obermayr, R., Dressler, K., Vrettos, C., & Eberhard, P. A calibration framework for DEM soil simulation and its application to a root growth model. Granular Matter, 13(6), 659–669, 2011.
[6] Li, B., Liu, F., Mu, J., Chen, J., & Han, W. Distinct element method analysis and field experiment of soil resistance applied on the subsoiler. International Journal of Agricultural and Biological Engineering, 7(1), 54-59, 2014.
[7] Huang, J., Godwin, R. J., & Kilic, E. Simulation of soil–tool interaction using discrete element modelling: A review. Soil & Tillage Research, 152, 125–137, 2016. https://doi.org/10.1016/j.still.2015.04.004
[8] Avdhoot Walunj, Saurabh Shinde, Sachin Nalawade, Pranav Pawase, Zhiwei Zeng, Effects of mouldboard shape and operational parameters on soil-ridger dynamics: An experimental and discrete element modelling approach, Smart Agricultural Technology, 12, 101250, 2025. https://doi.org/10.1016/j.atech.2025.101250.
[9] A. Walunj, Y. Chen, Y. Tian, Z. Zeng, Modeling Soil–Plant–Machine Dynamics Using Discrete Element Method: A Review, Agronomy 13 1260, 2023. https://doi.org/10.3390/agronomy13051260.
[10] Ucgul, M., Fielke, J. M., & Saunders, C. Three-dimensional discrete element modelling of tillage: Determination of a suitable contact model and parameters for a cohesionless soil. Biosystems Engineering, 121, 105–117, 2014. https://doi.org/10.1016/j.biosystemseng.2014.02.009
[11] Ucgul, M., Fielke, J. M., & Saunders, C. Simulation of tillage forces and soil movement using discrete element modelling: A review. Soil & Tillage Research, 144, 142–153, 2014. https://doi.org/10.1016/j.still.2014.07.010
[12] Ucgul, M., Fielke, J. M., & Saunders, C. Comparison of 3D discrete element modelling of a sweep tool with soil bin test results. Biosystems Engineering, 139, 82–93, 2015. https://doi.org/10.1016/j.biosystemseng.2015.08.001
[13] Li, H., Zhang, Y., He, Y., Wang, M., & Zhao, C. Discrete element simulation of soil cutting by inclined blades with bonded particle model. Advanced Powder Technology, 25(6), 1786–1794, 2014. https://doi.org/10.1016/j.apt.2014.06.001
[14] Deng, X., Chen, Y., Zhang, Q., & Sun, C. Calibration of DEM parameters for cohesionless and cohesive soils. Transactions of the ASABE, 59(3), 757–768, 2016.
[15] Fang, C., Zhang, Y., & Zhang, N. DEM simulation of soil particle movement and tool-soil interaction under different soil conditions. Transactions of the Chinese Society for Agricultural Machinery, 47(6), 41–49, 2016.
[16] Qi, H., Zhang, X., Li, X., Chen, Y., & Sun, H. Comparative study on angle of repose

test methods and the influence of moisture content on sandy clay soil. Soil & Tillage Research, 195, 104413, 2019. https://doi.org/10.1016/j.still.2019.104413

[17] Chen, Y., Liu, J., Lobb, D., & Tessier, S. Discrete element simulation of soil aggregation affected by tillage tools. Soil & Tillage Research, 134, 172–180, 2013. https://doi.org/10.1016/j.still.2013.08.009